Střelcová, K., Škvarenina, J. & Blaženec, M. (eds.): "BIOCLIMATOLOGY AND NATURAL HAZARDS"
International Scientific Conference, Poľana nad Detvou, Slovakia, September 17 - 20, 2007, *ISBN 978-80-228-17-60-8*

Impact of the biopores morphology on infiltration properties of soil

M. Sněhota [1], M. Sobotková [1], C. Ray [2] and M. Císlerová [1]

[1] Dept. of Irrigation, Drainage and Landscape Engineering, CTU in Prague, Czech Republic
(e-mail: michal.snehota@fsv.cvut.cz)

[2] Water Resources Research Center, University of Hawaii, U.S.A. (e-mail: cray@hawaii.edu)

Abstract Disturbances of soil structure, originated from biological activity, often represent potential pathways of the preferential flow. This study sums the results of experiments performed on five undisturbed soil columns, which were examined by the axial computed tomography (CT) and were the subject of the infiltration-outflow experiments. CT imaging was used to reveal the morphology of potential preferential pathways. The 3D reconstruction of biopore structure from CT images was done by means of segmentation based on the mathematical morphology operations pore erosion and dilation. The patterns of high porosity regions, which include also the empty biopores or biopores filled with loose material were reconstructed. The connectivity, total volumes and semivariograms of structures were analyzed in connection with the flow dynamics as monitored during infiltration-outflow experiments.

Key words: *preferential flow; flow patterns; biopores; x-ray computed tomography*

Introduction

Soil structure fundamentally affects the water flow and solute transport in soil profile. In structured and heterogeneous soils water is often conducted only by a small fraction of the soil volume but under substantially higher flow velocities when compared to the homogeneous soil matrix. The flow with high differences in local flow velocities and with occurrence of local nonequillibrium of pressures is called preferential flow. It was shown by various authors *(e.g. Vogel et al., 2000)* that flow and solute transport in heterogeneous soil media cannot be described satisfactorily by a standard single domain models based on the Richards equation. A new modelling approach based on dual permeability *(Gerke and Van Genuchten, 1993)*, which is suitable for mathematical description of the preferential flow and transport *(Dušek et al., 2006; Zumr et al., 2006)* has a very complex parameterization of the soil hydraulic properties. There is an aim to simplify the parameter estimation by supplying additional information about the fraction and characteristics of preferential flow domain. One of the most efficient methods, which are currently available for three-dimensional probing of a porous medium, is the X-ray computer axial tomography (CAT) or the computer tomography (CT). The method is based on the attenuation of x-ray or gamma beams in materials. The method was developed as a medical imaging technique *(Hounsfield, 1972)*. Because of the excellent ability to reveal the spatial distribution of the inner structure of three-dimensional objects, it became into the use in broad variety of the sciences.

The potential for determining the soil density distribution by the CT imaging was reported by *Hopmans et al.* (*1994*), who have demonstrated the capabilities and limitations of current medical scanners on two examples. In the first example, the spatial and temporal distribution of the tracer solute within the soil sample during infiltration and drainage was revealed by the CT. In the second example, variability of the distribution of soil density was derived from CT images of dry soil. A linear relationship between the CT absorption coefficient and the local bulk density was found. A linear relationship is also commonly used to derive the porosity from CT images (*Ashi 1997*).

Qualitative and quantitative evaluation of flow domains was done by *Kasteel et al. (2000),* who used local attenuation coefficients of the CT images to derive the hydraulic conductivity. They partitioned the volume of the undisturbed soil column into two material classes according to a fixed threshold evaluated from CT image. Hydraulic properties derived from the pore scale model were assigned to the material of lower density. Denser material was considered as non-desaturating under the condition of the experiment. The Ks values were distributed randomly between two materials in order to keep the known overall hydraulic conductivity. In the resulting 3D grid, the numerical simulation of solute transport was performed and the results were compared with the tracer experiment data. In a detailed study by *Císlerová and Votrubová, (2002)* the images obtained by CT were compared to images from magnetic resonance imaging (MRI) and dye tracer experiments. Undisturbed samples of coarse sandy loam and Dutch fine sand were studied. Sandy loam soil exhibited the preferential flow along the less dense regions. Preferential flow was observed also for Dutch fine sand, but its nature was different because in this case the denser regions have conducted the flow preferentially. For both soils, the porosity distribution was derived from the CT images. The difference in structure was demonstrated in semivariogram plots. The influence of slice orientation during CT imaging was also studied. It was found that the direction of scanning affects the image quality more than image resolution. The authors concluded that, for appropriate determination of flow domains in heterogeneous soil, the tresholding of CT data itself is not the sufficient information since the flow paths are not dependent only on local macroscopic porosity. MRI and dye tracing methods were recommended to obtain the additional information.
Current standard CT medical scanners are not suitable for the micro scale characterization of pore networks due to insufficient resolution. However, the imaging and reconstruction of the large macropores is feasible, and CT imaging seems to be a very efficient method to characterize macropore networks. *Perret et al., (1999)* non-destructively quantified the macropore networks in 3D. Based on CT images of long undisturbed samples of sandy loam, they quantified volume, wall area and hydraulic radius of all macropores with equivalent cylindrical diameter greater than 1 mm. *Pierret et al. (2002)* presented a similar study, where a new algorithm for the macropore tracing and visualization was used. The methodology was tested on two groups of undisturbed soil samples, where one group was taken from the site colonized by indigenous and in second one the earthworm specie were newly introduced. However, there was no significant difference observed between the samples, based on macropore geometry traced by CT.
Purpose of this study was to give an overview of methods of soil inner structure examination and to summarize the data which were obtained in experiments done on undisturbed soil columns of five soils. All soil samples were examined by the axial computed tomography (CT) and were also the subject of infiltration-outflow experiments.

Material and methods

Soil samples

An undisturbed soil core (189 mm diameter x 250 mm length) was collected from four experimental sites from mountainous areas of Czech Republic. The sample KH is a coarse sandy loam from Korkusova hut (Šumava Mountains, Long. 13°46', Lat. 49°01') experimental site (*Císlerová et al., 1988),* KR is a soil sample taken from Modrý Důl experimental watershed (Giant Mountains, Long. 15°43', Lat. 50°43'), UHL is a sample from the Uhlirska experimental watershed *(Šanda, et al. 2004)* (Jizera mountains Long. 15°09', Lat. 50°49') and LIZ is a soil core from the Liz experimental catchment (Šumava mountains, Long. 13°40', Lat. 49°04'). Contrasting soils series is represented by the soil core POA (size 142 mm diameter x 203 mm Length,), which is an Oxisol from Poamoho experimental site (Oahu, Hawaii, USA, Long. 158°05', Lat. 21°32') *(Snehota et al., 2007, Gavenda et al., 1996).*

Table 1: Description of the soil columns examined using x-ray tomography.

soil core	description	volume *(cm^3)*	bulk density *(g/cm^3)*
KH	Dystric Cambisol, B horizon, coarse sandy loam, 40-65 cm depth	7010.3	1.46
KR	soil from Cambisol series, sandy loam, B horizon, 20-45 cm depth	7010.3	0.89
LIZ	forest soil from Cambisol series, loamy sand, B horizon, 20-45 cm depth	7010.3	(-)*
JIZ	Soil from Cambisol series, "sandy loam", B horizon, 27-52 cm depth	7010.3	(-)*
POA	Oxisol of the Wahiawa series, silty clay, B horizon, 40-55 cm depth	3218.0	1.33

** soil cores LIZ and JIZ currently undergo experiments, therefore bulk density for these cores was not measured*

CT imaging background

The physical principle of the technique and the method of the image reconstruction are described elsewhere *(Duliu, 1999)*, so only a brief description will be given here. CAT maps show the distribution of linear attenuation coefficients over the entire transverse section. Once an X-ray beam of energy range 30 – 200 keV (the energy range of present-day tomographs) is penetrating the object, its interaction with the matter is given by three effects; coherent scattering, photoelectric and Compton (incoherent) scattering. In this range of energies the linear attenuation coefficient μ depends on the both, the effective atomic number Z_{ef} and the density ρ of the object. Attenuation of well-collimated X- or gamma ray follows the Beer's law:

$$I = I_0 \exp(-\mu x)$$

where I_0 is the integral current of incident *X* or gamma photons, I is the integral current transmitted by the sample, x is the sample width.

When the energy of the X-ray is higher then 100 keV the Compton effect prevails and the linear attenuation coefficient μ depends on the density of the sample but not on its chemical composition.

By measuring the attenuation of a thin beam of radiation, with the constant distance between the beam source and the detector, the product μx is determined. The attenuation is measured in a finite number of co-planar directions. By using the appropriate reconstruction algorithm, the matrix of linear attenuation coefficients is obtained. This represents the slice which thickness is roughly equal to the beam diameter.

The image intensities are usually expressed in Hounsfield units (HU), which is a convenient linear transformation of μ and is calibrated to obtain 0 HU for the air, and +1000 HU for water. In some scanners the HU value equal to zero is reserved for the image intensity of water.

Imaging of the soil samples using CT and the image processing

The samples were scanned on the standard medical CT equipment. The CT images of soil samples KH, LIZ, JIZ and KR were done using the medical scanner Siemens SOMATON PLUS IV. Files in IMA format were direct outputs of the imaging, each file containing one slice (in the x-y plane) composed of the matrix 512 x 512 pixels. The slice thickness was 1 mm for all the samples. The imaging step along the z-axis was 1mm. The field of view (FOV) was adjusted according to the sample dimensions. Soil sample POA was scanned in Toshiba Aquillion 16, CT scanner; slices were collected at the pace of 0.5 mm with the slice thickness of 0.5 mm. The matrix size was 512 x 512 and the final spatial resolution was 0.3315 x 0.3315 mm^2. The acquired data have been stored in DICOM format for further processing.

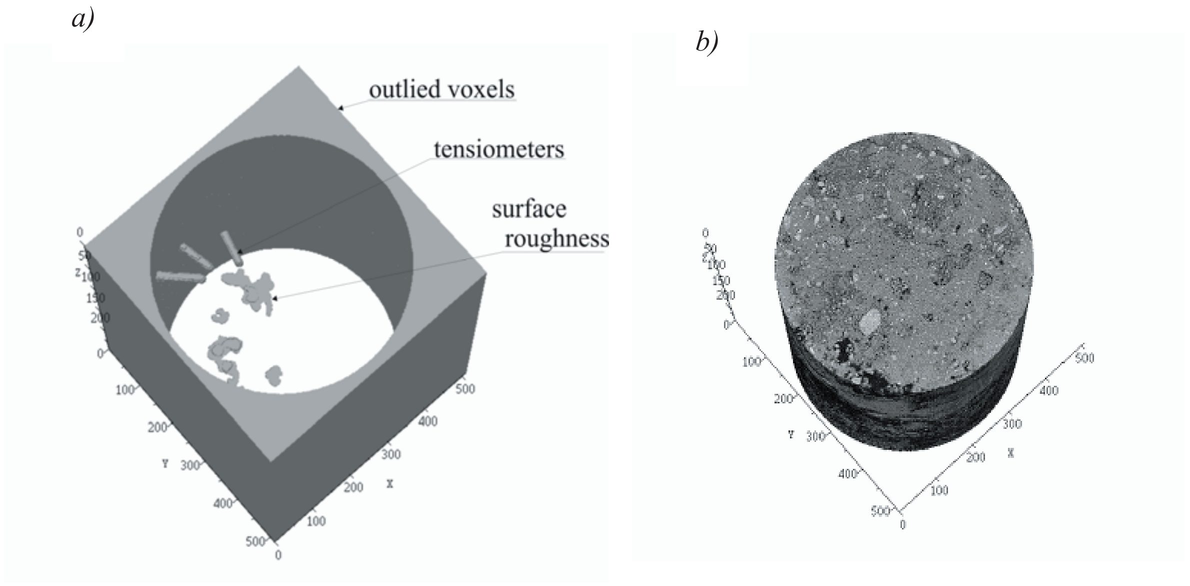

Figure 1 : Example of invalid (a) and valid (b) voxels of the soil sample KH

To prepare the images for quantitative evaluation the basic image-processing was conducted using auxiliary computer codes written in FORTRAN and MATLAB. Firstly, the images in IMA and DICOM formats were converted into binary data files. Then constant value of –100 HU was assigned to the voxels which apparently did not represent soil porous media. Outlier voxels and voxels, which belong to the space occupied by tensiometers, were considered invalid. Figure 1 shows an example of the separation between valid and invalid voxels.

Visualization of the soil inner structure by CT is an excellent source of qualitative information. However, the next step of CT images use is based on quantitative analysis. The mapping of macropore network geometry is the first type of a quantitative use. This is however possible only for large structures of the size sufficiently larger then the voxel size. The second type of information is given by the transformation between the image intensities and the macroscopic effective soil physical properties. This should be done with an extra care, considering possible errors. The bulk density and the porosity distribution can be derived from a CT image. Voxel densities can be calibrated from CT intensity values in case of a completely dry *(Hunt, 1988, Hopmans et. al, 1994, Císlerová a Votrubová 2002)* or a saturated sample *(Ashi, 1997)*. When a dry sample is considered, local density of each voxel can be estimated using linear relationship

$$\rho_{ikj} = a.i_{HUijk}$$

where: i_{HUijk} …… the attenuation of the voxel at i,j,k coordinate of the composite CT image (HU)
a ……. a coefficient

Coefficient a is obtained as

$$a = \frac{\rho_d}{\bar{i}_{HU}}$$

where $\bar{i}_{HU}$ ….. the mean attenuation of a whole sample CT image (HU)
ρ_d …... the bulk density

Estimation of the porosity distribution is based on a presumption of the constant particle density. Then the relationship for the porosity of voxel i,j,k is assumed to be

$$n_{ijk} = 1 - \frac{\rho_{d\,ijk}}{\rho_s}$$

where ρ_s……… the particle density
ρ_{ijk}……… the soil bulk density in the voxel i,j,k derived from the image intensity

It is often not possible to dry the soil core properly prior to the CT imaging, since it would damage the soil. Then the x-ray beam is also attenuated by the present pore water which then increases the measured values of HU. The total amount of water is known but the correction is not feasible, since the water content distribution is unknown. Even when the earlier described approach to the porosity calculation diminishes the present water induced error on the mean porosity estimate, the local values of porosity stay affected. The error is minimized when the water content is very low. Alternative approach is the scanning of a soil sample under the full water saturation. In the present study the POA soil core was scanned at full water saturation. Therefore its HU values were shifted by +1000 HU. The shift was later removed in order to allow the comparison of the POA sample results with the rest of the soil samples, which were scanned at low water contents.
A modified method based on the morphological operation of pore opening described in detail by *Vogel, (1997)* was employed in this study to discriminate and visualize the potential preferential pathways. The pore opening, which is a combination of morphological erosion and dilation, has been mostly used for discrimination of pores at the micro-scale *(Vogel and Roth, 2001)*, or for characterization of large macropores *(Capowiez et al., 2006)*. In this study the same approach was applied to perform the segmentation of regions with certain HU values, which are sufficiently low to be considered as highly conductive for water. In this approach two conditions must be fulfilled, the HU values must be lower than a given threshold value and the region size must be larger or equal then the size of structuring element. Not only macropores/biopores but also highly porous structures are considered as potential preferential pathways.

Infiltration-outflow experiments

Besides the CT scanning the five soil cores were also the subject of infiltration outflow experiments. With controlled boundary conditions the experiment on large undisturbed soil core is a promising tool to estimate the soil hydraulic properties *(Robovská, 2000),* and to monitor flow deviations. In the present study, this experiment was used to detect the preferential flow.

Results

The inner structure of five soil columns was revealed from CT images. The example of one image slice is shown in Figure 2.

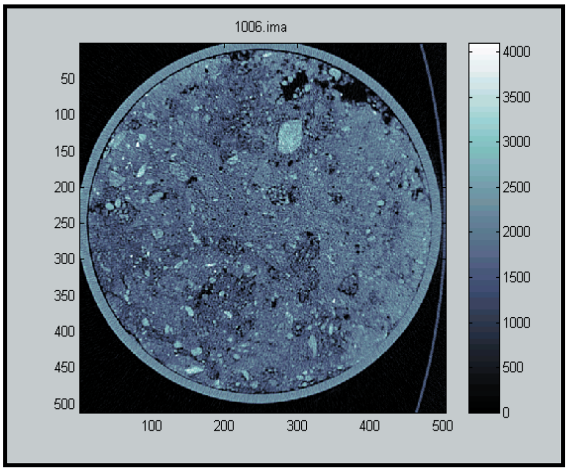

Figure 2: Example of one image slice (soil sample KH). Image intensities are in HU units.

Figure 3 shows the CT images of five soil columns. The 3D images were reconstructed from individual slices and outlier voxels were removed.

In the next step the pore opening was performed on the CT 3D images. The example of the result is shown in Figure 4 for the soil cores UHL and LIZ. Significant differences between the soil structure of the both cores is evident. The soil core LIZ contains a much higher number of interconnected regions of the high porosity which may represent preferential pathways. The high porosity patterns found for the sample UHL are less pronounced.

In addition to the qualitative evaluation of the CT information, a semivariogram analysis was conducted to quantify the vertical and horizontal continuity of high porosity regions. This geostatistical technique can be used to characterize and describe the spatial correlation of phenomena that are spatially distributed. In the case of detected high porosity regions it may help to determine whether a potential preferential flow pattern may exist. The semivariogram analysis was conducted on segmented images. An example of semivariogram is shown in Figure 5 for the soil core KH. The semivariogram was calculated for the selected 3D matrix 312 x 312 x 226 voxels. The vertical continuity of high density regions, which in case of the soil core KH originated most probably in earthworm activity, was detected by the semivariogram.

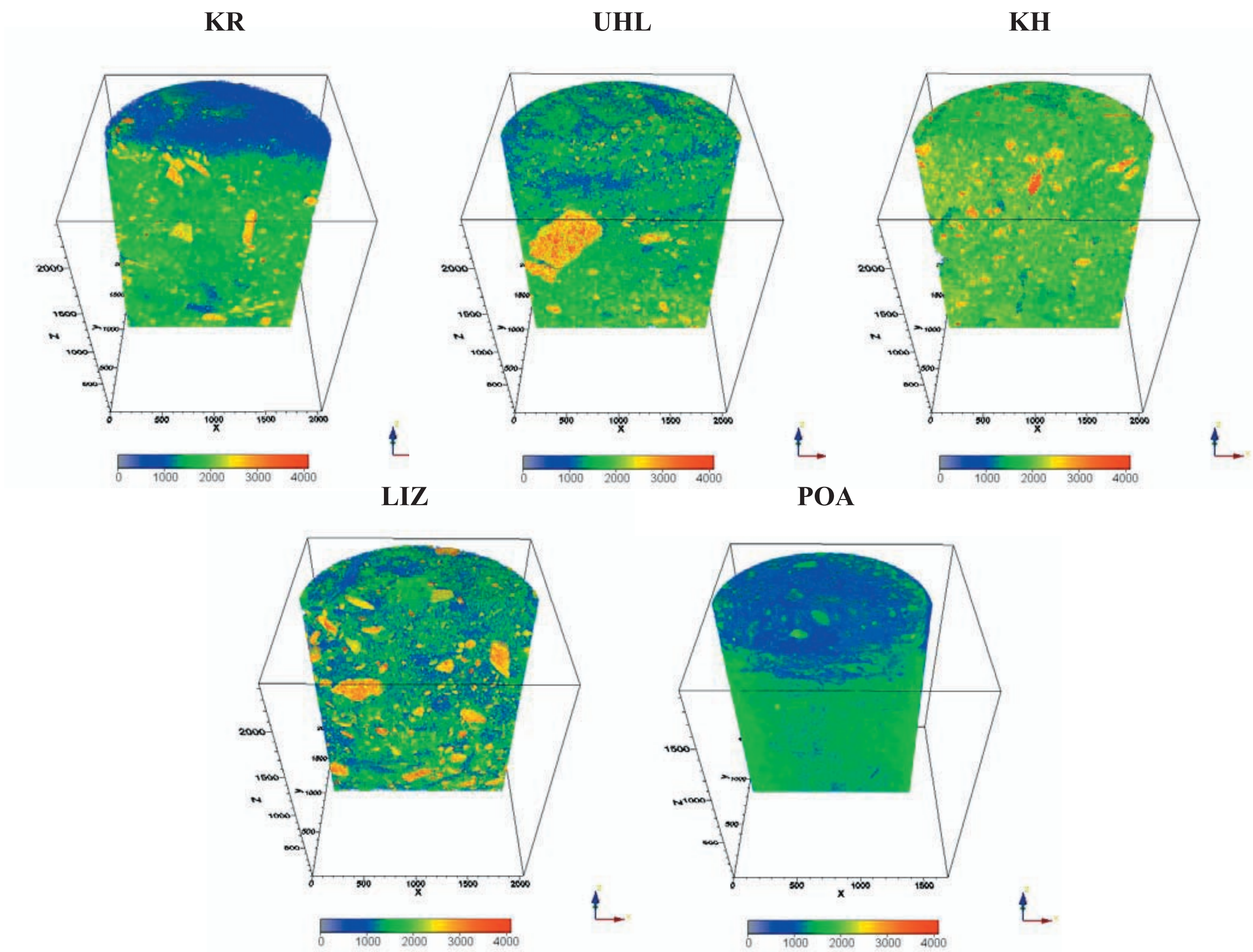

Figure 3: Reconstructed 3D CT images of five soil column. The front part of the soil sample was removed. Colour scale, which is the same for all images, represents the HU values. The spatial scale of the images is the same for all images except of the POA sample, which was smaller.

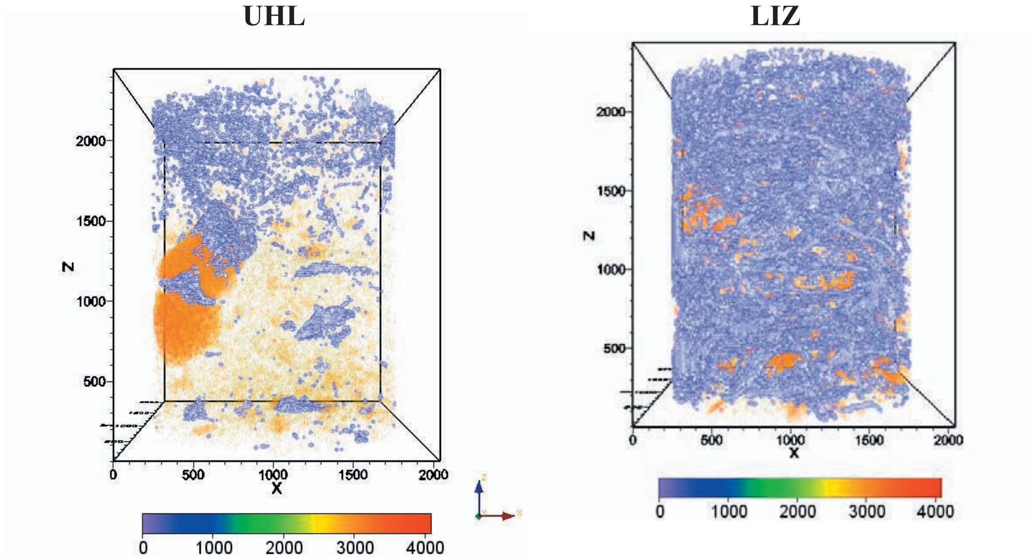

Fig. 4: 3D reconstructed CT images of potential preferential pathways (blue). Objects with HU < 1000 and the equivalent radius of at least 2 mm are visible. The image shows also the densest parts (stones) of the soil (orange).

a)

b)

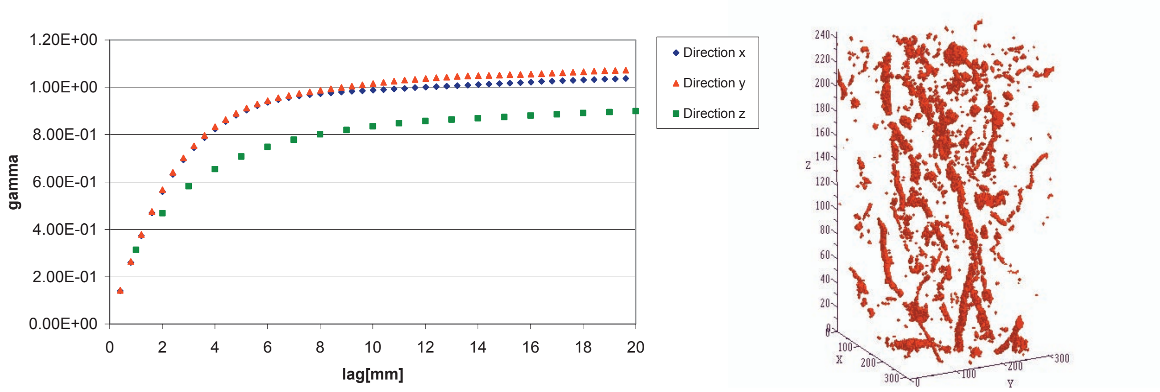

Fig. 5: Semivariogram (a) based on 3D matrix 312 x 312 x 226 voxels (b) of segmented image data (soil sample KH). Lower value of gamma in z direction clearly shows the vertically elongated shape of regions of high porosity.

Infiltration experiments

Infiltration experiments have been conducted on five soil columns obtaining cumulative water fluxes across top and bottom boundaries and pressure data from tensiometers recorded in time. A series of infiltrations have been conducted at each soil core with different pressures heads maintained at the top of the column. In Figure 6 and Figure 7 the examples are shown for the soil columns KH and KR. Several features can indicate the existence of the preferential flow. When water flows preferentially, the outflow starts very early and outflow flux density is initially low. As the infiltration proceeds, the outflow rate slowly increases until the moment when infiltration and outflow rates equal and a steady state flow is reached (see Figures 6b and 7b). This phenomenon is not present when infiltration is done under lower pressure heads maintained at the sample top when preferential pathways become non effective (see Figures 6a and 7a) or in soils without preferential flow. Another indicator of the preferential flow is the pressure records measured by tensiometers.

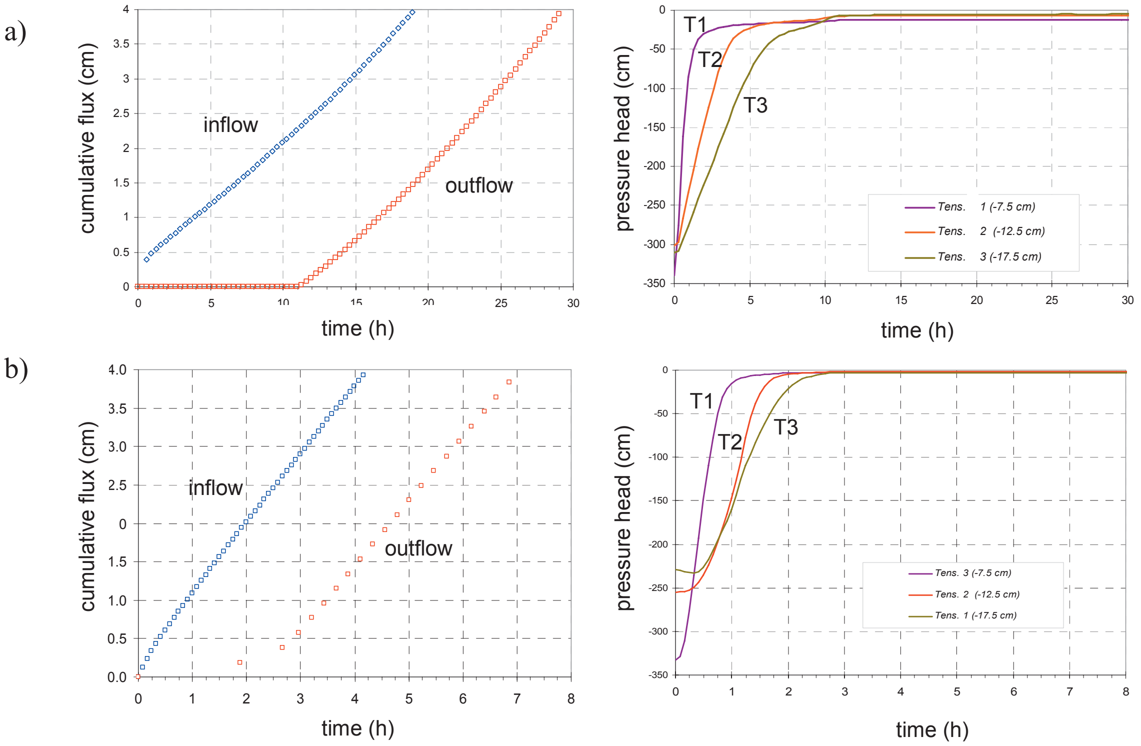

Figure 6: Results of the infiltration experiment on soil core KH. Cumulative infiltration and outflow (left) and pressure heads measured in three tensiometers (right). Infiltration under (a) -6 cm and (b) -1cm pressure head at the top. (Snehota et al. 2002).

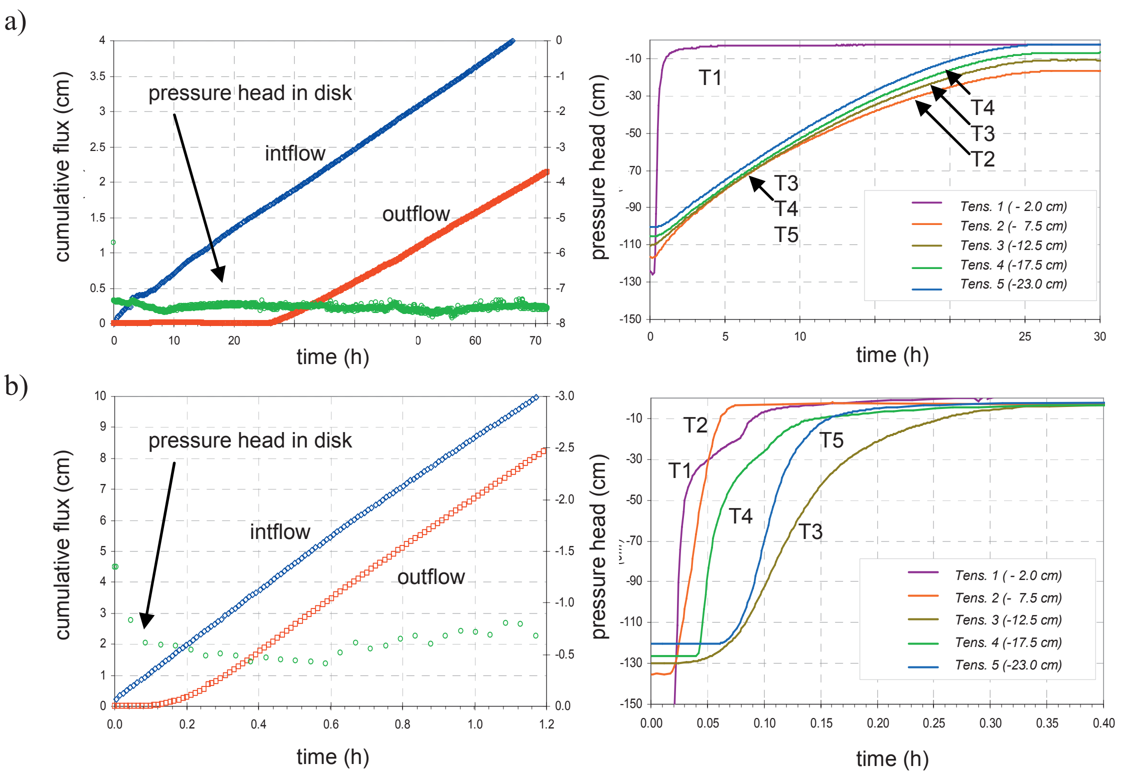

Figure 7: Results of the infiltration experiment on soil core KR. Three infiltrations with pressure head (a) -3 cm and (b) -1cm. Cumulative infiltration and outflow (left) and pressure heads measured in five tensiometers (right). (Snehota et al. 2005).

Conclusion

The purpose of this contribution is to present a method used in an ongoing research on detection and quantification of preferential flow in soils. Other complementary experiments, e.g. dye tracer experiments *(Zumr et al., 2007)* or breakthrough curve experiments *(Sobotkova et al., 2007)* targeted on the preferential flow detection and the detection of other flow deviations are running simultaneously. Results of the infiltration experiments proved that the preferential flow was present in three soil cores. In the soil core from Oxisol series the preferential flow was less pronounced. Infiltration experiments on the soil from Jizera Mountains are currently in progress. It was found that the potential preferential pathways, detected by non-invasive CT imaging, varied significantly for the studied soil samples, even though the soil cores were taken from the same soil series. The summary of experimental results will be given in detail at the conference presentation.

Acknowledgements

This research has been supported by Ministry of Education of the Czech Republic, project no. MSMT 1K05024.

References

[1] Ashi, J. 1997. Computed tomography scan image analysis of sediment. In Shipley, T.H., Ogawa, Y., Blum, P., and Bahr, J. M.(Eds.) *Proceedings of the Ocean Drilling Program, Scientific Results* Vol. 156, Texas A&M University 151-159.

[2] Capowiez, Y., Bastardiea, F., Costagliola, G. 2006 Sublethal effects of imidacloprid on the burrowing behaviour of two earthworm species: Modifications of the 3D burrow systems in artificial cores and consequences on gas diffusion in soil. *Soil Biology & Biochemistry* 38, 285–293

[3] Císlerová, M., J. Simunek, T. Vogel, 1988. Changes of steady state infiltration rates in recurrent ponding infiltration experiments. *Journal of Hydrology*, 104:1-16.

[4] Císlerová, M. and Votrubová, J. 2002. CT derived porosity and flow domains. *Journal of Hydrology* 267: 186-200.

[5] Duliu, O.G., 1999. Computer axial tomography in geosciences: an overview. *Earth-Science Reviews*, 48(4): 265-281.

[6] Dušek, J., T. Vogel, L'. Lichner, A. Čipáková and M. Dohnal, Simulated cadmium transport in macroporous soil during heavy rainstorm using dual-permeability approach. *Biologia,* 61 (Suppl. 19): 251-254.

[7] Gavenda, R.T., Green, R.E., and Schneider, R.C., Leaching of pesticides in selected Hawaii Oxisols and Andisols as influenced by soil profile characteristics, *HITAHR Research Series 075, University of Hawaii at Manoa,* HI, U.S.A., 1996.

[8] Gerke, H. H. and van Genuchten, M. Th. 1993. A dual-porosity model for simulating the preferential movement of water and solutes in structured porous media. *Water Resour. Res*. 29[2]: 305-319.

[9] Hopmans, J.W., Cislerová, M., and Vogel, T., 1994. X-Ray Tomography of Soil Properties. In: *Tomography of Soil-Water-Root Processes, SSSA Special publication no. 36*. SSSA, Madison.

[10] Hounsfield, G. N. 1973. Computerized transverse axial magnetic resonance scanning (tomography): I. description of system. *Br. J. Radial.* 46: 1016-1022.

[11] Hunt, K., Engler, P., and Basjsarowicz, C. 1988. Computed tomography as a core analyses too: applications, instrument evaluation, and image improvement techniques. *Journal of Petroleum Technology* 9: 1203-1210.

[12] Kasteel, R., Vogel, H.J., and Roth, K. 2000. From local hydraulic properties to effective transport in soil. *European Journal of Soil Science* 51: 81-91.

[13] Perret, J., Prasher, S.O., Kantzas, A., and Langford, C. 1999. Three-Dimensional Quantification of Macropore Networks in Undisturbed Soil Cores . *Soil Sci. Soc. of Am. J.* 63: 1530-1543.

[14] Pierret, A., Capowiez, Y., Belzunces, L., and Moran, C.J., 2002. 3D reconstruction and quantification of macropores using X-ray computed tomography and image analysis. *Geoderma*, 106 (3-4): 247-271.

[15] Robovská, A., 2000. Measurements of hydraulic characteristics using tension disc infiltrometer on large soil samples. (In Czech). *PhD. Thesis, CTU in Prague*

[16] Snehota, M., M. Dohnal, M. Cislerova. and M. Tesař, 2005, Large undisturbed soil samples from two mountain watersheds: Infiltration experiments and imaging by means of computer tomography (in Czech), *proceedings of the conference Hydrologie malého povodí 2005*. Prague.

[17] Snehota, M., Ray, C., Lichwa, J., Sobotkova, M., 2007, Leaching of pesticides in tropical soils – column study, *Final report for HDOA, WRRC, University of Hawaii at Manoa*, HI, U.S.A.

[18] Sobotková, M., M. Sněhota, M. Císlerová, 2007. The effect of initial water saturation on the solute transport, *Geophysical Research Abstracts*, vol. 9, 00888.

[19] Šanda, M., T. Vogel, M. Císlerová, M. 2004. Euromediterranean Conference. Hydrograph formation in the hillslope transect. *Progress in Surface and Subsurface Water Studies at the Plot and Small Basin Scale*, Turin, Italy.

[20] Vogel, H.J., 1997. Morphological determination of pore connectivity as a function of pore size using serial section. *European Journal of Soil Science*, 48:365-377.

[21] Vogel, H. J. and K. Roth, 2001, Quantitative morphology and network representation of soil pore structure, *Advances in Water Resources*, 24, 3-4, 233-242.

[22] Vogel, T., Gerke, H.H., Zhang, R. and van Genuchten, M. Th.. 2000. Modeling flow and transport in a two dimensional dual-permeability system with spatially variable hydraulic properties, *J. Hydrol.*, 238, 78-89.

[23] Zumr D., M. Dohnal, M. Hrnčíř, M. Císlerová, T. Vogel, F. Doležal, 2006. Simulation of soil water dynamics in structured heavy soils with respect to root water uptake. *Biologia,* 61 (Suppl. 19): 320-323.

[24] Zumr, D. 2007 Monitoring the preferential flow in heterogeneous soils by dye tracers. *(in this issue)*